CO_2-Expanded Alkyl Lactates: A Physicochemical and Molecular Modeling Study

Yaocihuatl Medina-Gonzalez[1,2] · Ahmed Jarray[1,2] · Séverine Camy[1,2] · Jean-Stéphane Condoret[1,2] · Vincent Gerbaud[1,2]

Abstract With the perspective of finding alternative benign media for various applications, this paper presents a study of the physicochemical behavior of some members of the alkyl lactate family when expanded by CO_2. Experimental and molecular modeling techniques have been used to determine and/or predict relevant physicochemical properties of these systems such as swelling, Kamlet–Taft parameters {polarity/polarizability (π^*) and proticity or hydrogen-bond donator ability (α), dielectric constants and solubility parameters}. To complete the study of these properties, sigma profiles of the three lactates molecules have been obtained by performing quantum mechanical and phase equilibria calculations of CO_2/alkyl lactate systems by using the Peng–Robinson equation of state.

Keywords CO_2 expanded liquids · Alkyl lactates · Green solvents · Green solvent engineering

1 Introduction

Environmental regulations all around the world respond to an increasing interest of the society for greener chemical processes. This green chemistry and engineering approach prompts the scientific community to propose innovative solutions to industrial problems and to consider aspects such as environmental toxicology and biodegradability with increased interest. One of the fields that present problems in most chemical processes is the use of solvents as almost all reaction chemistry happens in solution. It is not surprising that

✉ Yaocihuatl Medina-Gonzalez
yaocihuatl.medinagonzalez@ensiacet.fr

[1] LGC (Laboratoire de Génie Chimique), CNRS, 4 Allée Emile Monso, BP 84234, 31030 Toulouse Cedex 4, France

[2] UPS, INSA, INPT; LGC (Laboratoire de Génie Chimique), Université de Toulouse, 31077 Toulouse, France

one of the twelve principles of Green Chemistry is the utilization of safer solvents. One of the approaches to fulfill these needs is the substitution of highly pollutant solvents by environmentally friendly, less toxic compounds, together with an effort to efficiently use these solvents.

Bio-derived solvents have attracted recent interest because of their low carbon footprint and their potential to be safer, more biodegradable and less toxic [1]. In this context, alkyl lactates are a group of biodegradable and non-toxic compounds, able to replace traditional toxic solvents because of their excellent solvent properties [2, 3]. As examples, ethyl lactate has recently been used in the 1,3-dipolar cycloaddition reaction and the synthesis of spiro-oxindole derivatives with excellent yields [4], the ligand-free Suzuki–Miyaura reaction has been performed in ethyl lactate with good yields [5] and aryl aldimines have been synthesized from aryl amines and aryl aldehydes in ethyl lactate without the need for a catalyst by using water as cosolvent [6].

From the perspective of finding alternative benign media to perform chemical reactions, gas-expanded liquids (GXLs), and more specifically CO_2-expanded liquids (CXLs), are very promising since they present several advantages such as: (1) being able to solubilize more solutes than their supercritical fluid counterparts, which is advantageous to dissolve catalysts and reactants; (2) CO_2 can be used to tune the power of the solvent across a large polarity range; and (3) GXLs can allow the combination of chemical reaction and product separation [7–9].

In this context, this work presents a study of the physicochemical behavior of some members of the alkyl lactate family when expanded by CO_2. The physicochemical parameters that have been experimentally studied are swelling (by using in situ FTIR spectroscopy), and the Kamlet–Taft parameters: polarity/polarizability (π^*) and proticity or hydrogen-bond donator ability (α) (by using solvatochromic compounds and in situ UV–Vis spectroscopy). Molecular dynamics (MD) simulations have been performed in the CXLs alkyl lactates in order to obtain the dielectric constants and the solubility parameters of these systems. Sigma profiles of the three alkyl lactate molecules have been obtained by performing quantum mechanical calculations. To complete this study, phase equilibria of CO_2/alkyl lactates have been calculated using the Peng–Robinson equation of state.

2 Materials and Methods

2.1 Reagents

Methyl, ethyl and butyl lactates (purities of 98%, ≥98% and 98% respectively), as well as the solvatochromic compound Nile Red (purity >98%), were purchased from Sigma–Aldrich and used as received. CO_2 with purity of 99.995% was purchased from Air Liquide.

The high-pressure variable-volume view cell (9.6–31.3 cm^3, Top Industrie, France) used in this study was equipped with three sapphire windows and a magnetic stirrer. The temperature of the cell was maintained at 313 K by a thermostatted bath and measured by a thermocouple (J type, precision of ±0.1 K) placed inside of the cell. Pressure was measured by a digital manometer (Keller, LEX 1, precision: 0.01%), equipped with a numerical pressure display. The cell was coupled to an FTIR (Fig. 1a) or a UV–Vis spectrophotometer (Fig. 1b) in order to obtain measurements for swelling or deriving π^* and α parameters as described in the next sections.

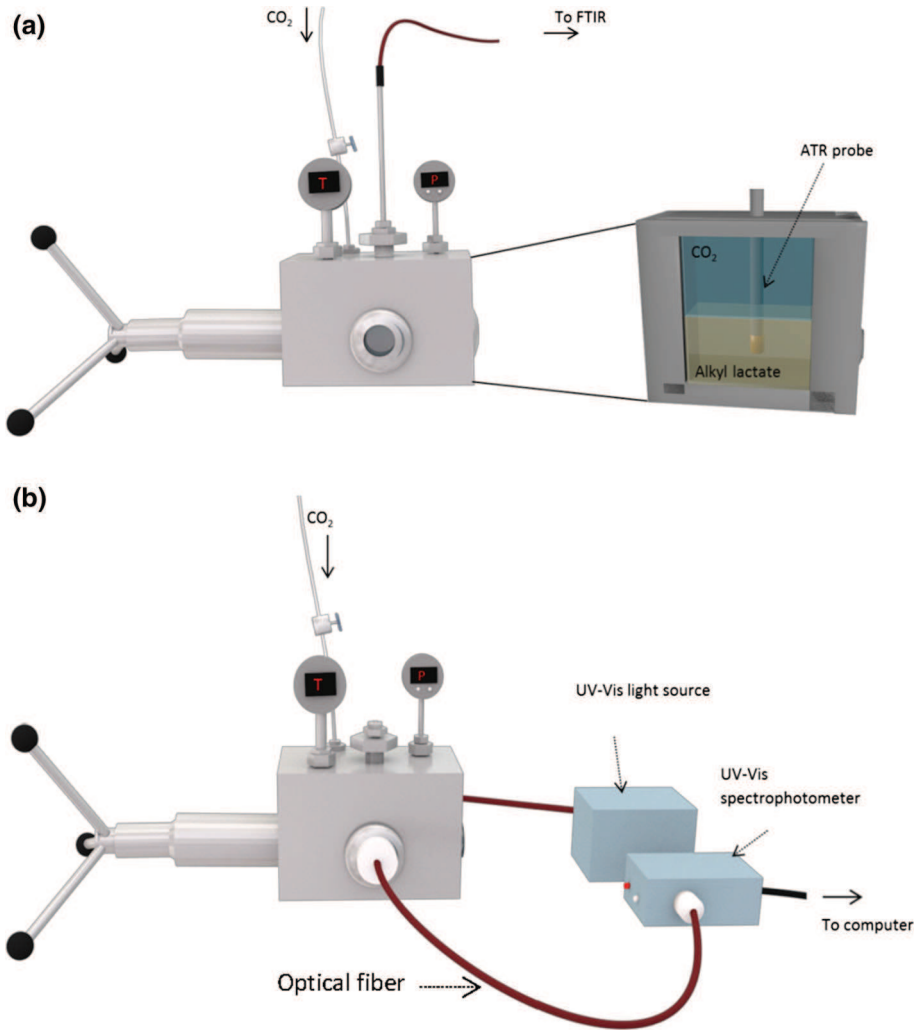

Fig. 1 Setup used in FTIR (**a**) and UV–Vis (**b**) determinations showing the high-pressure view cell coupled to the respective spectrophotometers. The enlarged feature on the right side in **a** shows the ATR probe immersed in the alkyl lactate phase

2.2 Swelling

A Bruker Tensor 27 FTIR Spectrometer, equipped with a high-pressure probe that performs measurements by ATR, was used for swelling determinations. Calibration curves of the three studied lactates have been performed in CCl_4 and obtained by solubilizing defined quantities of alkyl lactates in this solvent and then recording their FTIR spectra. This curve allowed determination of the concentration of alkyl lactate in the alkyl lactate phase, which was used to obtain the swelling results [10].

Density determinations were performed as follows: the view cell was filled with the alkyl lactate and flushed with CO_2, then tightly closed. The temperature was fixed at 313 K

and maintained by the thermostatted bath; the contents of the cell were agitated by a magnetic stirrer. CO_2 was injected with the aid of an ISCO high-pressure syringe pump until the desired pressure inside the cell was reached; at this point, we used a video camera to ensure that the ATR probe was well immersed in the liquid solvent-rich phase. The pressure range for these experiments was chosen to be between 10 and 80 bar in order to insure a biphasic system, from the knowledge of phase equilibria of binary systems (see phase equilibrium calculations section).

For calculations, the Beer–Lambert law {$A = \varepsilon \cdot L \cdot c$, where A is the sample absorbance, ε the molar extinction coefficient ($L \cdot mol^{-1} \cdot cm^{-1}$), L the optical path length (cm) and c the sample concentration ($mol \cdot L^{-1}$)}, and the calibration curve were used to calculate the concentrations of alkyl lactate in the alkyl lactate-rich phase. The band observed at 1730 cm^{-1} for the alkyl lactates and attributed to C=O stretching was recorded as the CO_2 pressure was increased in order to calculate the concentration of lactate in the lactate-rich phase and then to calculate the swelling of the alkyl lactate by CO_2. Each spectrum was acquired at 30 min of interval and equilibrium was judged as reached when at least three spectra were identical.

Peak height instead of peak area was used for these determinations in order to minimize the error. Swelling of the alkyl lactate-rich phase (S) has been calculated as the ratio between the initial concentration of alkyl lactate (C_0) in the alkyl lactate-rich phase to its concentration (C) at a given CO_2 pressure [$S = (C_0/C) - 1$]. By taking into account all the sources of errors associated with our methodology, a maximum error of about $\pm 5\%$ was estimated.

The densities of the lactates at $p = 0$ (where p is the pressure of CO_2) bar have been obtained by this method and compared with literature values, showing good agreement.

2.3 Solvatochromism

Different measures of polarity can be used to compare solvents. For gas-expanded liquids, Kamlet–Taft parameters present great interest as they can be used to differentiate acidity (α, ability to donate a proton in a solvent–solute hydrogen bond) from basicity (β, ability to accept a proton in a solvent–solute hydrogen bonding), from dipolarity/polarizability (π^*, ability to stabilize a charge or dipole). CO_2 has very low Kamlet–Taft parameters and, as it dissolves in liquids, the polarity of the solvents changes depending on the nature of the liquid.

The solvatochromic behavior of CO_2-expanded methyl, ethyl and butyl lactates was determined at various CO_2 concentrations by using Nile Red (NR) as a solvatochromic compound. A solvatochromic experiment probes the solvation effect on the electronic transition energy of a photochromic molecule, denoted by the wavelength or wavenumber at maximum absorption (λ_{max} or υ_{max}, respectively) [11]. It is important to note that solvatochromic probes characterize the local environment, meaning the cybotactic area of the probe, which may differ from the values of the bulk solution. However, the different species solubilized in a gas-expanded liquid may experience the local effects of polarity, which are observed by using solvatochromic probes [12].

The UV–Vis spectrometer used for determination of Kamlet–Taft parameters was a StellarNet Inc. EPP2000 equipped with optical fibers and an Ocean Optics DH-2000 light source. Solvatochromic determinations were performed as follows: the view cell was filled with an alkyl lactate and with Nile Red as the solvatochromic molecule, flushed with CO_2 and then tightly closed. The temperature of 313 K was kept constant by the thermostatted bath and the content of the cell was agitated by a magnetic stirrer. CO_2 was then injected

by the aid of an ISCO pump until the desired pressure was reached inside the cell. A reference spectrum was obtained for the pure alkyl lactate. UV–Vis spectra were acquired in the same pressure ranges as the FTIR. The average of 200 spectra was used for calculation of the Kamlet–Taft parameters.

2.4 Phase Equilibrium Calculations

Phase equilibria data of CO_2/alkyl lactate binary mixtures at 313 K have been performed using Simulis® Thermodynamics (Prosim S.A. France) software in the Excel (Microsoft) environment, using literature data. Cho et al. [13, 14] have obtained experimental fluid phase equilibria of methyl through butyl lactates with CO_2 in the temperature range from 323 to 363 K, and correlated them with the well known PR EoS [15] using the van der Waals (vdW) one-fluid and the Wong–Sandler (WS) mixing rules. Although they showed that the WS mixing rules allowed a better representation of experimental data for the methyl and ethyl lactate systems, the vdW one-fluid mixing rules have proven to give acceptable predictions for the lactate family. Because of the lack of experimental data describing critical properties (T_c, p_c) and acentric factor (ω) of lactates, they used several group contribution methods to estimate these properties and compared their modelling results to experimental ones in order to select the most suitable method. Their studies showed that best results were obtained with parameters predicted by the Nannoolal–Rarey (T_c and p_c) and Lee–Kesler (ω) methods. Pure component properties necessary for the PR EoS and used in this study are reported in Table 1. Binary interaction parameters for the vdW one-fluid mixing rule obtained by Cho et al. and used in this study are reported in Table 2.

The results of Cho et al. [13, 14] show that the solubility of CO_2 in the alkyl lactate phase increases as the size of the alkyl lactate hydrocarbon chain increases. The extent of the diphasic zone is indeed lower for CO_2/butyl lactate than for CO_2/ethyl lactate, which is in turn lower than for the CO_2/methyl lactate system. Experimental results were correlated in a satisfying way using PR calculations, the highest discrepancies are observed at high temperature near the critical point of the mixtures. PR predictions tend to show that solubility of lactate in the CO_2 phase slightly increases in the order methyl > ethyl > butyl.

Table 1 Critical properties and acentric factor of pure compounds used in the PR EoS (data taken from Cho et al. [13, 14])

	T_c (K)	p_c (bar)	ω
CO_2	304.21	73.83	0.2236
Methyl lactate	629.5	37.1	0.312
Ethyl lactate	633	33.4	0.348
Butyl lactate	660.04	27.6	0.420

Table 2 Binary interaction parameters used in PR EoS with vdW one-fluid mixing (data taken from Cho et al. [13, 14])

	CO_2/methyl lactate	CO_2/ethyl lactate	CO_2/butyl lactate
k_{ij}	0.0709	0.0526	0.047

The PR EoS has been used in our study to predict fluid phase equilibria of CO_2/alkyl lactates binary systems at 313 K, as in previous studies performed by Cho et al. [13, 14], and also at temperatures of 323 K and higher.

2.5 Molecular Modeling

2.5.1 Sigma Profile

The Conductor-like Screening Model (COSMO), implemented in the Dmol^3 module as a part of Material Studio 7.0 package of Biovia (2013), was used to generate the sigma profiles of the three molecules (butyl lactate, methyl lactate and ethyl lactate). Water was chosen as the solvent environment (relative dielectric constant = 78.54). A global orbital cutoff radius of 3.7 Å was used throughout the calculations. We have used the local PWC functional representation of Perdew and Wang [16] for the COSMO calculations. It has been demonstrated by Perdew and Wang that this technique produces more reliable predictions than the Vosko–Wilk–Nusair (VWN) technique [17]. The Ortmann–Bechstedt–Schmidt (OBS) scheme [18] was employed for correction of the damped atom-pairwise dispersion which is suitable for PWC and covers all the elements of our studied molecules. In Dmol^3-COSMO (Biovia 2013), the charge density is represented by molecular shaped cavities. The radii of the spheres that make up the cavity surface were determined as the sum of the van der Waals radii of the atoms of the molecule and of the probe radius. For best accuracy, we used the triple-numerical polarization (TNP) basis set [19]. Geometry optimization was performed first to bring the energy to a stationary point and to adjust the coordinates of the atoms. Then, molecular dynamic simulations were performed over 0.25 ps (250 steps) with a time step of 1 fs at the canonical NVT ensemble. The temperature was set at $T = 298.15$ K and controlled by using the massive generalized Gaussian moments thermostat. The sigma profiles were averaged over the last resulting 10 fs.

2.5.2 Molecular Dynamics

Molecular dynamics calculations were performed using the Forcite module included in the Materials Studio 7.0 software from Biovia. A typical simulation box at the beginning consisted of 2000 molecules, but, after several determinations, the number of molecules was decreased to 400 without noticeable change in the results, so the rest of the calculations have been performed with boxes containing 400 molecules. This size is a compromise between cells being large enough for minimal volume effects and being small enough for an efficient computational treatment. Our approach is similar to that of Gohres et al. [20], where instead of simulating a multiphase system, a microscopic volume of the GXL was modeled by MD. The appropriate conditions for this modeling, such as composition, temperature and pressure, have been obtained from the PR EoS phase equilibrium calculations and from experimental data. The simulations reported here were performed in the isothermal–isobaric ensemble (NPT) at the temperature 313 K using a Nosé–Hoover thermostat with a thermostat mass $Q = 0.01$ and at different pressures; pressure was controlled by a Berendsen barostat. Cubic periodic boundary conditions were applied and long-range interactions treated using the Ewald summation method. Four different force fields available in the Materials Studio software were used in this study in order to compare the obtained results: COMPASS II, Dreiding, pcff and the universal force field (UFF). Geometry optimization was performed on the initially constructed boxes. After an

equilibration period of 50 ps or more, until the energy and density of the systems remained constant, a production dynamics simulation was performed for 200–3000 ps. Trajectory data were collected in 50 ps blocks and averaged to estimate the uncertainties, presented as error bars (5%).

Cohesive energy density (E_{CED}) calculations were performed as well by using the Forcite Module in Materials Studio, using the same force field as in the molecular dynamics simulation. E_{CED} represents the energy needed to completely remove a unit volume of molecules from their neighbors to infinite separation (ideal gas), meaning that E_{CED} is a measure of the intermolecular forces within a system and is estimated via the non-bonded van der Waals and electrostatic (including hydrogen bond) interactions [21]:

$$E_{CED} = \frac{U_{vdw} + U_Q}{vM} \tag{1}$$

where U_{vdw} and U_Q are, respectively, van der Waals and electrostatic energy; the solubility parameter (δ) can be expressed as:

$$\delta = \sqrt{\delta_{vdw}^2 + \delta_Q^2} \tag{2}$$

where δ_{vdw} and δ_Q represent, respectively, the contributions from van der Waals forces and electrostatic interactions and:

$$\delta_Q = \sqrt{E_Q} = \sqrt{\frac{U_Q}{vM}} \tag{3}$$

$$\delta_{vdw} = \sqrt{E_{vdw}} = \sqrt{\frac{U_{vdw}}{vM}} \tag{4}$$

where E_Q is the electrostatic energy density and E_{vdw} is the van der Waals energy density. As it can be seen, the solubility parameter has dispersion and electrostatic components. These contributions, together with hydrogen bonding, are frequently used to assess the compatibility of solvents and solutes.

The relative permittivity (ε_r) was calculated from the average fluctuations in the total dipole moment using the formula [22, 23]:

$$\varepsilon_r = 1 + \frac{\langle M^2 \rangle - \langle M \rangle^2}{3\varepsilon_0 V k_B T} \tag{5}$$

where M is the total dipole moment, V is the volume of the simulation box, k_B is the Boltzmann constant, ε_0 is the vacuum permittivity and T is the temperature. The angled brackets represent ensemble averages. The total dipole moment is given by the following equation:

$$M = \sum_{i=1}^{N} q_i r_i \tag{6}$$

where q_i is the partial charge of atom i and r_i is the distance of that atom from a fixed origin. In this study, partial charges have been assigned by the force field. In the case of COMPASS II, these charges have been parameterized by using ab initio electrostatic potentials. UFF was developed in combination with the QEq charge equilibration method.

Molecular dynamics calculations where performed by using the OCCIGEN supercomputer (Bull cluster, 2.1 PFLOPS) from the Centre Informatique National de l'Enseignement Supérieur (CINES) at Montpellier, France.

3 Results and Discussion

3.1 Liquid–Vapor Modeling

Liquid–vapor equilibrium determination is crucial when studying gas-expanded liquids as the bubble point represents the solubility of the gas in the liquid phase. Some experimental studies are available in the literature concerning CO_2/alkyl lactates, however not all data are available at the temperature and pressure ranges used in our study so we performed calculations of fluid phase equilibria at 313 K for the systems studied by us using the PR EoS and the results are presented in Fig. 2.

Phase diagrams shown in Fig. 2 confirm the trend of CO_2 mol fraction in lactates, at a given pressure (i.e., solubility of CO_2), as being the highest for butyl lactate and the lowest for methyl lactate, whereas the solubility of alkyl lactate in CO_2 varies in the opposite trend. Whatever the considered lactate, at 313 K binary systems are completely monophasic, no matter the mixture composition, at pressure above 83–84 bar.

3.2 Swelling

Swelling behavior of gas-expanded liquids strongly depends on the nature of the studied liquid. As the gas dissolves into the liquid, the volume of the liquid phase expands, and this expansion significantly affects the physicochemical properties of the liquid phase.

FTIR spectra obtained during swelling experiments are presented in Fig. 3 for the three lactates studied. As can be observed, because of the CO_2 solubilization in the alkyl phase, the band attributed to C=O stretching decreases as the pressure increases, causing alkyl lactates to swell in the presence of CO_2.

3.3 Solvatochromism

Typical behavior of the normalized absorption spectra of NR in neat lactates and in CO_2-expanded alkyl lactates is exemplified by the spectra obtained for methyl lactate at

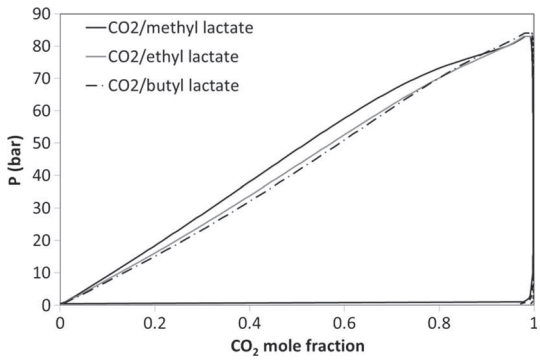

Fig. 2 CO_2/alkyl lactates binary phase diagram at 313 K obtained with PR EoS

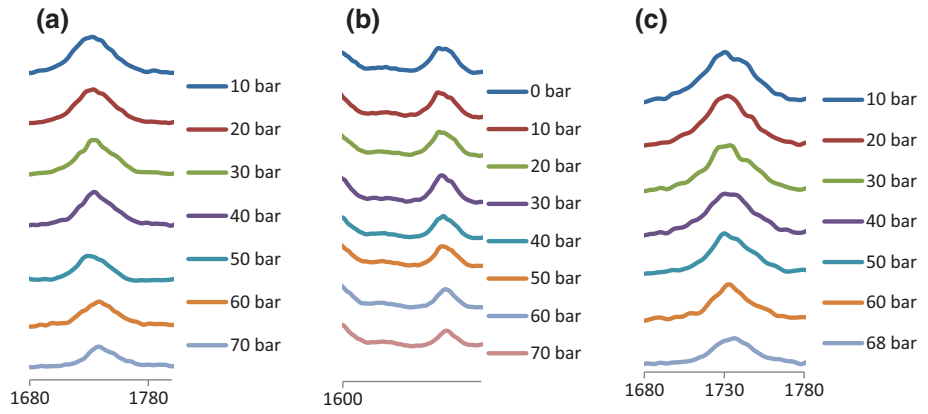

Fig. 3 FTIR changes in alkyl lactates spectra with the CO_2 pressure: **a** methyl lactate, **b** ethyl lactate, and **c** butyl lactate

Fig. 4 Normalized absorbance spectra of CO_2-expanded methyl lactate at different relative pressures, $T = 313$ K

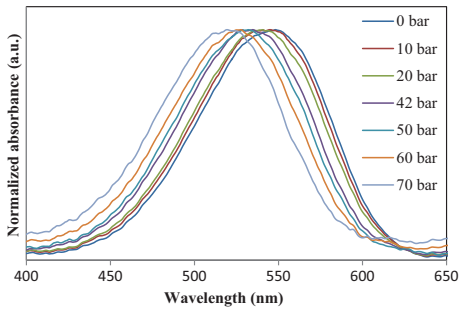

different CO_2 pressures as shown in Fig. 4. The spectra obtained consist of one peak in the visible region that keeps the same shape over the entire range of CO_2 pressures that correspond to dissolved CO_2 concentrations in the solvent. Indeed, the dissolved CO_2 concentration increases when the CO_2 pressure increases. As CO_2 is added, the peak undergoes a hypsochromic shift, as expected from the fact that the polarity of the alkyl lactate decreases with increasing CO_2 concentration.

The λ_{max} value for the absorption maximum of the spectra of Nile Red in pure and in CO_2-expanded alkyl lactates was used to calculate the Kamlet–Taft π^* and α parameters by using Eqs. 7 and 8 [24, 25]. As expected, the polarizability and hydrogen-bonding donating ability parameters of CO_2-expanded alkyl lactates decrease as the CO_2 concentration increases. As is well known, Nile Red dye is strongly sensitive to the polarity and hydrogen bonding donor ability of the solvent, showing a bathochromic shift in the absorbance when these two characteristics increase [26]. Inversely, when these two parameters decrease, a hypsochromic shift is observed as given by:

$$\lambda_{max} = 19.993 - 1.725\pi^* \tag{7}$$

$$\lambda_{max} = 19.9657 - 1.0241\pi^* - 1.6078\alpha. \tag{8}$$

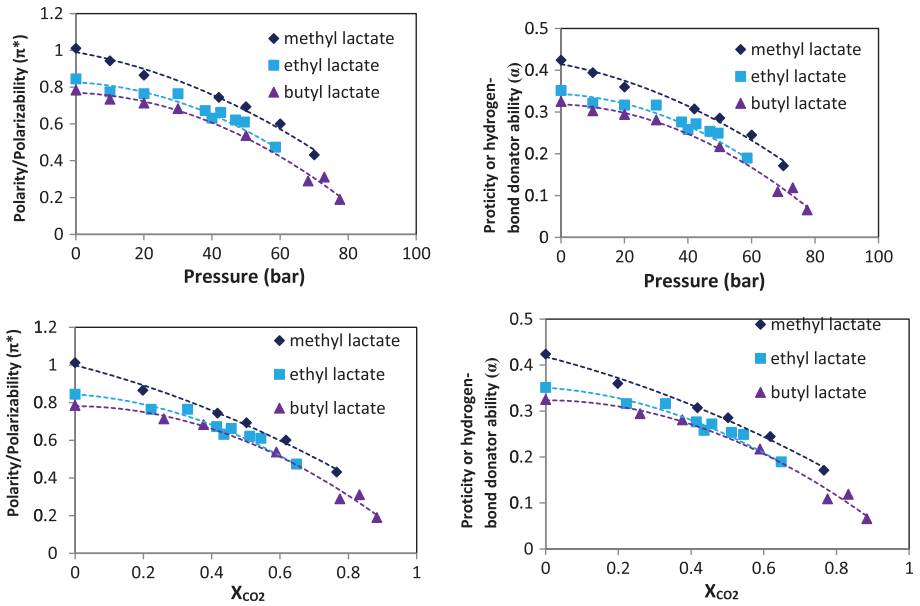

Fig. 5 Kamlet–Taft π^* and α parameters for the three alkyl lactates studied as functions of the CO_2 pressure and mole fraction

As observed in Fig. 5, the π^* and α values of the solvent phase decrease with an increase of the CO_2 pressure, hence with its dissolved concentration, suggesting that polarity/polarizability and proticity or hydrogen-bond donating ability decrease for the three lactates. As it is well known, alkyl lactate structures are characterized by the vicinity of hydroxyl and carbonyl groups that gives rise to remarkable intramolecular hydrogen bonding when the hydroxyl group is in the molecular plane in the gas phase. However, in a liquid phase, the greater molecular flexibility allows the hydroxyl group to move out of the molecular plane, permitting intermolecular hydrogen bonding [2, 27], and the presence of CO_2 in the lactate phase decreases its possibility to create intermolecular hydrogen bonds, as is well observed in the experimental results. Values obtained for both parameters are presented in Table 3.

3.4 Molecular Modeling

3.4.1 Sigma Profiles

The 3D molecular surface polarity distributions resulting from quantum chemical calculations can be visualized in Fig. 6a. Figure 6b shows a histogram function, called sigma profiles, of butyl lactate, ethyl lactate and methyl lactate. In general, the COSMO histogram is qualitatively divided into three regions with the following cutoff values: hydrogen bond donor region ($\sigma < -1$ e·nm^{-2}), non-polar region ($-1 < \sigma < 1$ e·nm^{-2}), and hydrogen bond acceptor region ($\sigma > -1$ e·nm^{-2}). As can be observed, the three alkyl lactate molecules have a major nonpolar peak, exemplified by the peak centered at zero screening charge density, and a small shoulder in the positive region of the σ-profile, meaning that they act as H-bond acceptor and are available for a H-bond donor. In

Table 3 Values obtained for the Kamlet–Taft π^* and α parameters for the three alkyl lactates/CO_2 systems

p^a (bar)	X_{CO_2}	π^*	α
CO_2/methyl lactate			
0	0	1.0115	0.4240
20	0.1987	0.8647	0.3600
42	0.4175	0.7443	0.3075
50	0.5018	0.6933	0.2853
60	0.6181	0.6003	0.2447
70	0.7660	0.4311	0.1800
CO_2/ethyl lactate			
0	0.0000	0.8448	0.3513
20	0.2227	0.7646	0.3163
30	0.3297	0.7646	0.3163
38	0.4148	0.6728	0.6728
40	0.4361	0.6315	0.2583
42.5	0.4575	0.6625	0.6625
46.9	0.5115	0.6212	0.6212
49.5	0.5445	0.6108	0.6108
58.6	0.6483	0.4739	0.1896
CO_2/butyl lactate			
0	0.0000	0.7847	0.3251
20	0.2602	0.7138	0.2942
30	0.3765	0.6831	0.2808
50	0.5896	0.5375	0.2173
73	0.8328	0.3117	0.1189
68.2	0.7757	0.2898	0.1093
77.5	0.8840	0.1897	0.0657

[a] p is the pressure of CO_2

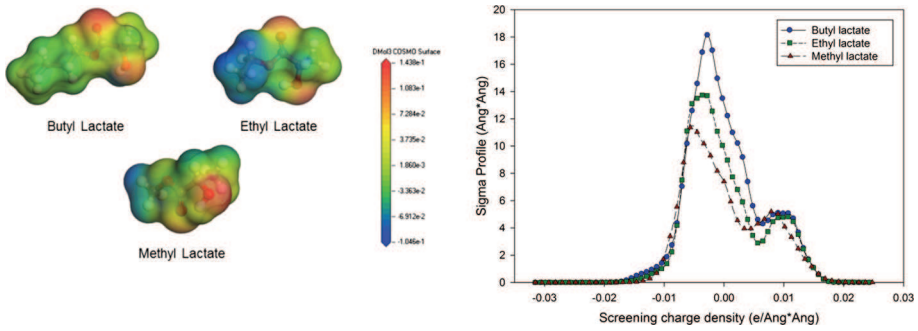

Fig. 6 Dmol^3-COSMO surfaces and sigma profiles of butyl, ethyl and methyl lactates

addition, the sigma profile of the nonpolar part of the molecule presents the tendency: butyl lactate > ethyl lactate > methyl lactate, which is confirmed by the solvatochromic measurements where polarity shows the tendency: methyl lactate > ethyl lactate > butyl lactate (Fig. 5).

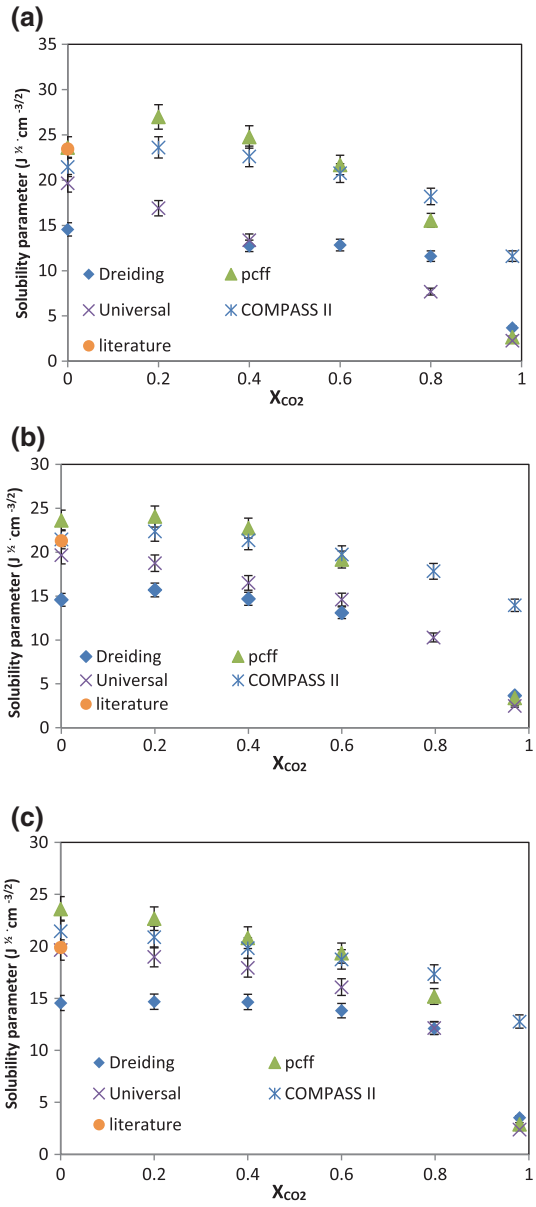

Fig. 7 Solubility parameters of **a** CO_2/methyl lactate, **b** CO_2/ethyl lactate and **c** CO_2/butyl lactate mixtures, obtained from cohesive energy density calculations from molecular mechanics simulations by using different force fields. Literature data for pure lactates are taken from Lomba et al. [29]

3.4.2 Molecular Dynamics

Figure 7 reflects the range of modulation of the solubility parameter of the CO_2-expanded alkyl lactates by controlling the CO_2 pressure. Almost 95% of the liquids, pure lactates, have solubility parameters that are between those of C_6H_{12} (16.8 $MPa^{1/2}$) and CH_3OH (29.3 $MPa^{1/2}$) [28]. Even though there are differences between the force fields used to

Table 4 Solubility parameter values of the three systems studied, as obtained from cohesive energy density calculations from molecular mechanics simulations by using different force fields. Literature data for pure lactates are taken from Lomba et al. [29], $T = 313$ K

X_{CO_2}	p (bar)	COMPASS II	Dreiding	pcff	Universal	Literature
CO_2/methyl lactate						
0	10	21.4619	14.5618	23.6098	19.6567	23.46
0.2	21	23.6207	–	26.9908	16.9067	–
0.4	41	22.6223	12.7453	24.7821	13.3796	–
0.6	59	20.7789	12.8399	21.6768	–	–
0.8	72	18.1979	11.5999	15.5563	7.6899	–
0.98	83	11.6081	3.6950	2.6599	2.2820	–
CO_2/ethyl lactate						
0	10	21.4619	14.5617	23.6098	19.6566	21.3
0.2	18	22.3704	15.7014	24.0606	18.7388	–
0.4	37	21.3544	14.6855	22.7301	16.5045	–
0.6	55	19.7309	13.0979	19.1575	14.6011	–
0.796	70	17.8163	–	–	10.2838	–
0.97	83	13.9429	3.6531	3.3999	2.4743	–
CO_2/butyl lactate						
0	10	21.4619	14.5618	23.6098	19.6567	19.9
0.2	15	20.9057	14.6821	22.6744	18.9960	–
0.4	32	19.8372	14.6569	20.8382	17.9462	–
0.6	51	18.7543	13.8261	19.3588	16.0843	–
0.798	70	17.3555	12.1219	15.1913	12.1625	–
0.98	84	12.7717	3.5458	2.9016	2.3996	–

calculate the solubility parameters, all of them predict a decrease of this parameter from its initial value at $X_{CO_2} = 0$ (pure lactate) as the pressure increases. Tables 4 and 5 present the values obtained for solubility parameter and density by using different force fields. Experimental values of density are reported in Table 6.

Figure 8 shows the comparison between density results from molecular mechanics calculations, using the different force fields available in the Materials Studio software, with experimental results obtained by FTIR measurements. As can be easily observed, the UFF calculations show good agreement with experimental results for the three alkyl lactates/CO_2 systems tested over all of the CO_2 concentrations and hence the pressure range. The Pcff force field describes well the experimental results in the cases of ethyl and butyl lactate/CO_2 systems. However, the methyl lactate/CO_2 system is not as well described with this force field. In the three systems studied, the Dreiding force field does not show good accuracy in the prediction of the density of the expanded phase. The UFF shows better results for the quantitative description of the density for the three studied CO_2-expanded alkyl lactates. It is worth noting, however, that even if not all the force fields used in this study give satisfactory results from a quantitative point of view, all of them show a decrease in the density of the expanded phase so this method might still be used for qualitative analysis of these fluids (Table 5).

Table 5 Density values ($g \cdot mL^{-1}$) obtained by MD calculations by using different force fields of the three studied systems at 313 K. Literature data are taken from Lomba et al. [29]

X_{CO_2}	p (bar)	COMPASS II	Dreiding	pcff	Universal	Literature
CO_2/methyl lactate						
0	1	1.065	0.824	1.094	0.926	1.071
0.2	21	1.065	0.738	1.081	0.909	–
0.4	41	1.06	0.812	1.049	0.876	–
0.6	59	1.046	0.786	0.954	0.799	–
0.8	72	0.994	0.688	0.71	0.478	–
0.98	83	0.76	0.221	0.19	0.171	–
1	100	0.709	0.275	0.222	0.203	0.6317
CO_2/ethyl lactate						
0	1	1.012	0.807	1.031	1.014	1.012
0.2	18	1.015	0.807	1.023	1.023	–
0.4	37	1.017	0.804	0.998	1	–
0.6	55	1.012	0.79	0.922	0.931	–
0.796	70	0.975	0.716	0.709	0.708	–
0.97	83	0.807	0.248	0.204	0.183	–
1	100	0.709	0.275	0.222	0.203	0.6317
CO_2/butyl lactate						
0	1	0.963	0.794	0.961	0.921	0.963
0.2	15	0.97	0.798	0.961	0.917	–
0.4	32	0.974	0.799	0.948	0.905	–
0.6	51	0.976	0.795	0.911	0.869	–
0.798	70	0.96	0.752	0.753	0.696	–
0.98	84	0.787	0.241	0.198	0.181	–
1	100	0.709	0.275	0.222	0.203	0.6317

Standard deviation for each value are less than 0.01

3.5 Swelling

The swelling behavior of the three studied alkyl lactate/CO_2 systems is shown in Fig. 9a. As can be observed, swelling that is directly related to density passes through a minimum for ethyl and butyl lactates, a phenomenon that is not observed for methyl lactate. This behavior can be related to the increase in the density of ethyl and butyl lactates for low concentrations of CO_2, and then to an expansion for higher concentrations of CO_2. This phenomenon is observed as well in the swelling behavior, which is negative at low CO_2 pressures. This behavior has also been observed before in acetonitrile, *N*,*N*-dimethylformamide and methanol [28]. We explain this behavior because, at low pressures, CO_2 can be accommodated in the existing free volume of the liquid solvent, increasing in this way its density, but at high pressures and high concentrations, CO_2 can no longer enter the solvent in this way and so causes an expansion of the solvent, thereby decreasing its density. The degree of the initial increase of the liquid solvent density strongly depends on the nature of the solvent. In our study, it can be observed that the longer is the hydrocarbon chain, the more pronounced is this behavior; thus, the increase in density at low CO_2 pressures follows the tendency butyl > ethyl > methyl. As Li and Maroncelli [28] have

Table 6 Experimental density values obtained for the CO_2/methyl lactate, CO_2/ethyl lactate and CO_2/butyl lactate mixtures at 313 K

p (bar)	X_{CO_2}	Density ($g \cdot mL^{-1}$)
CO_2/methyl lactate		
1	0.0000	1.0700
10	0.0995	0.9908
20	0.1987	0.9197
30	0.2971	0.9133
40	0.3971	0.8728
50	0.5018	0.7867
60	0.6181	0.6496
70	0.7660	0.4952
CO_2/ethyl lactate		
0	0.0000	1.0160
10	–	1.0369
20	0.2227	1.0378
30	0.3297	0.9538
40	0.4361	0.9361
50	0.5445	0.8643
60	0.6605	0.7805
70	0.7961	0.6396
CO_2/butyl lactate		
0	0.0000	0.9670
10		1.1133
20	0.2602	1.0242
30	0.3765	0.9739
40	0.4856	0.9069
50	0.5896	0.8701
60	0.6916	0.7618
70	0.7979	0.6013

Calculated uncertainties are about ±10%. Values of X_{CO_2} was obtained from PSRK calculations

suggested, expanded solvents cannot be considered as fluids with larger molar volumes or lower densities than conventional solvents, but may be rather considered as fluids with more free volume than the original liquids. We can add to this statement that the hydrocarbon chain length plays a key role in volumetric expansion and consequently in density changes for gas-expanded liquids. This behavior is reinforced as well by the solubility of CO_2 in the alkyl lactate phase calculated by EoS and from literature data, which follow the tendency butyl > ethyl > methyl, meaning that a better solubilization of CO_2 favors an increase in density. Table 7 shows the values obtained for swelling for each studied CO_2/alkyl lactate system.

To reinforce these observations, we have calculated the packing fraction (f_{occ}) [28] as the ratio of the van der Waals (V_{VdW}) volume occupied by the molecules in the modelization box to the molar volumes obtained by MD calculations with UFF (Eq. 9, Fig. 9b). Van der Waals volumes of the molecules were calculated by Bondi's method [31] (Table 8). The decrease of the packing fraction across all the pressure range is related to the increase in free volume; this decrease is more pronounced for butyl and ethyl lactates than for methyl lactate,

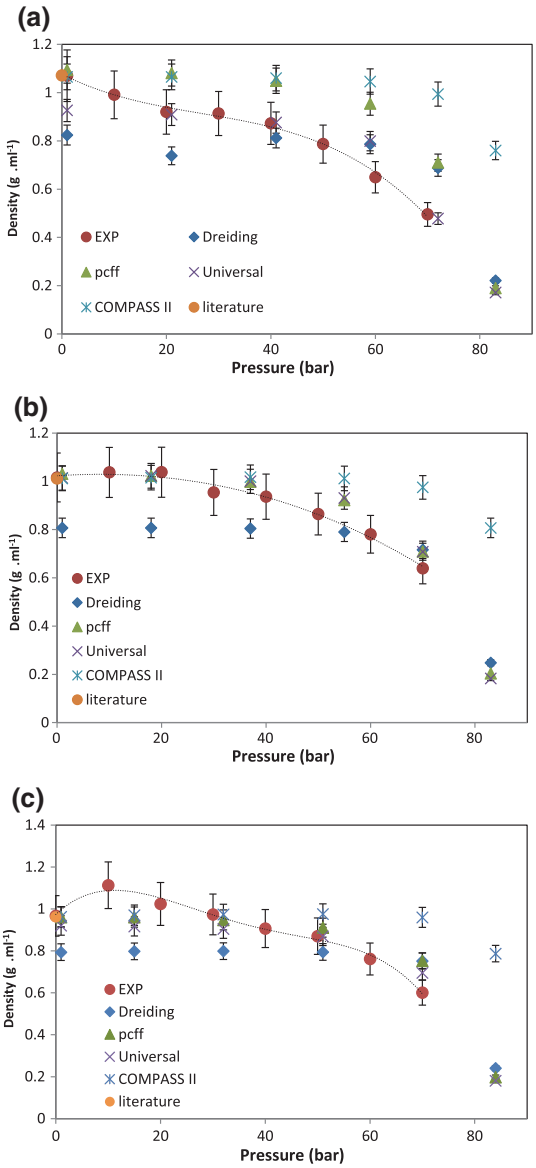

Fig. 8 Density of the **a** CO_2/methyl lactate, **b** CO_2/ethyl lactate and **c** CO_2/butyl lactate mixtures at 313 K obtained from MD calculations by using different force fields and comparison with experimental results. Literature data have been taken from Lomba et al. [29, 30]. *Lines* have been added to guide the eye

$$f_{\mathrm{occ}} = \frac{\sum_{i=1}^{n} V_{\mathrm{VdW}}}{V_{\mathrm{MD}}} \tag{9}$$

where n is the number of molecules in the box. Obtained values of f_{occ} are reported in Table 9.

Figure 10 shows the dependence of solvent polarity on pressure, from molecular mechanics calculations using different force fields. Rather than plotting the permittivity (ε_r), we plot here the polarization or reaction field factor, calculated as:

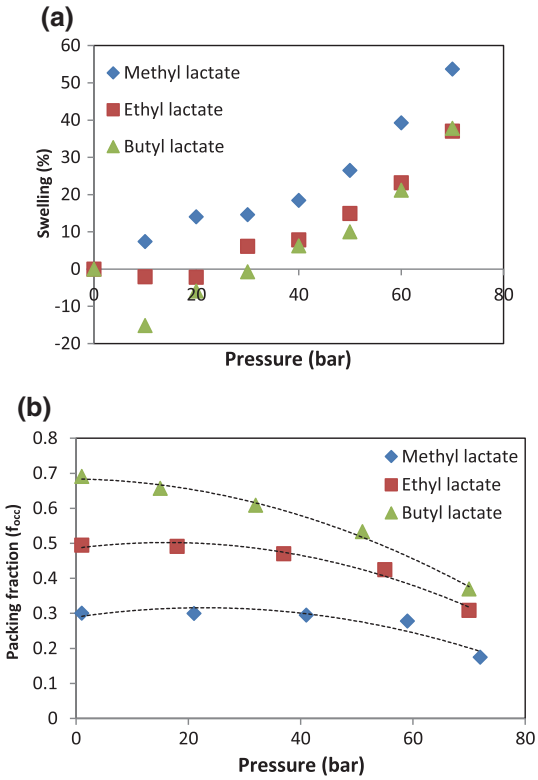

Fig. 9 **a** Swelling of the CO_2/alkyl lactate mixtures at 313 K obtained from experimental results, and **b** packing fractions obtained from density calculations by using UFF. *Lines* have been added to guide the eye, $T = 313$ K

Table 7 Swelling (in %) of the alkyl lactates/CO_2 mixtures at 313 K obtained from experimental results

p (bar)	CO_2/methyl lactate	CO_2/ethyl lactate	CO_2/butyl lactate/CO_2
0	0	0	0
10	7.3987	−2.0613	−15.1261
20	14.0478	−2.1491	−5.9113
30	14.6445	6.1182	−0.7124
40	18.4323	7.8595	6.2195
50	26.4749	14.9270	10.0187
60	39.2912	23.1797	21.2164
70	53.7160	37.0512	37.8129

Table 8 VdW volumes calculated for the studied molecules

Molecule	VdW volume ($cm^3 \cdot mol^{-1}$)
CO_2	17.587
Methyl lactate	47.36
Ethyl lactate	57.59
Butyl lactate	78.05

Table 9 Packing fractions obtained from density calculations by using UFF at 313 K

p (bar)	V_m ($cm^3 \cdot mol^{-1}$)	VdW vol ($cm^3 \cdot mol^{-1}$)	f_{occ}
CO_2/methyl lactate			
1	157.8618	47.3600	0.3000
21	138.3344	41.4054	0.2993
41	120.2192	35.4508	0.2949
59	106.2303	29.4962	0.2777
72	134.8201	23.5416	0.1746
CO_2/ethyl lactate			
1	116.4990	57.5900	0.4943
18	100.9834	49.5894	0.4911
37	88.4820	41.5888	0.4700
55	79.1171	33.5882	0.4245
70	83.5176	25.7476	0.3083
CO_2/butyl lactate			
1	113.0293	78.0500	0.6905
15	100.4166	65.9574	0.6568
32	88.4685	53.8648	0.6089
51	78.3038	41.7722	0.5335
70	80.6727	29.8005	0.3694

$$f(\varepsilon_r) = \frac{\varepsilon_r - 1}{\varepsilon_r + 2}. \tag{10}$$

The reaction field due to polarization by the equilibrium dipole moment is proportional to $f(\varepsilon_r)$; this reaction field factor is used here since it is commonly used to relate solvation energies to solvent permittivity and is more relevant to solvatochromism than is ε_r [28], as solvatochromic shifts observed in dye molecules are due to variations in the solvent reaction field. As can be observed in Fig. 10, a strong "dielectric non ideality" is present in the expanded alkyl lactate phases, exemplified by the nonlinear dependence of the reaction field factor with CO_2 composition [28], implying that solvation energies will be nonlinear functions of the composition of these phases. Table 10 gives values of reaction field factor obtained for the three studied systems.

In order to observe the evolution of hydrogen bonding between lactate molecules with CO_2 molecules, we have computed the radial distribution functions of pure butyl lactate and of the butyl lactate/CO_2 system ($X_{CO_2} = 0.6$) by taking into consideration the distance between the hydrogen of the hydroxyl group and the double bonded oxygen of lactate (Fig. 11). Destruction of intermolecular hydrogen bonds was observed in the butyl lactate/CO_2 system in contrast with pure alkyl lactate. This result agrees with experimental determinations of α (hydrogen-bond donator ability) by solvatochromism, where a decrease of this parameter is observed with CO_2 solubilization in the alkyl lactates.

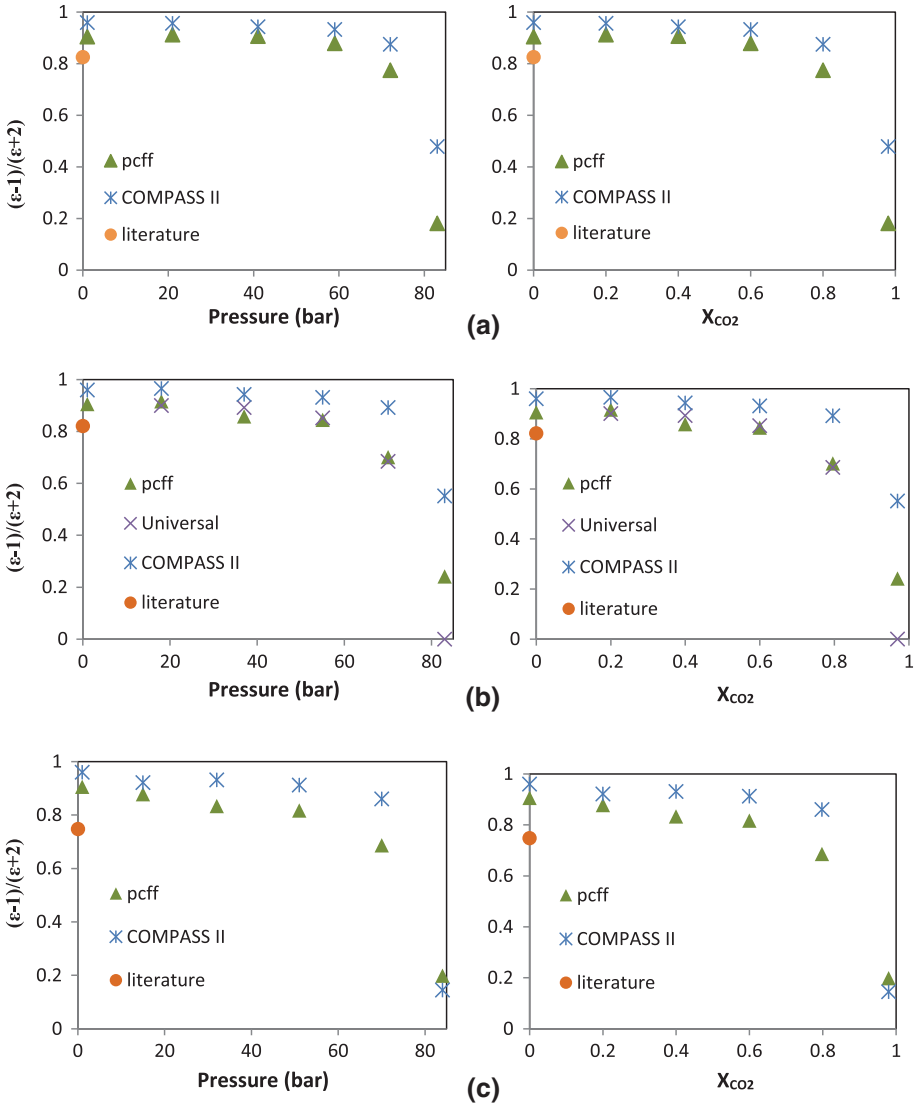

Fig. 10 Reaction field factor $(\varepsilon - 1)/(\varepsilon + 2)$ of the **a** CO_2/methyl lactate, **b** CO_2/ethyl lactate and **c** CO_2/butyl lactate mixtures at 313 K; the values of ε have been obtained from MD calculations by using different force fields

Table 10 Reaction field factor $(\varepsilon - 1)/(\varepsilon + 2)$ of the three studied systems at 313 K; ε values are from MD calculations by using different force fields

X_{CO_2}	p (bar)	COMPASS II	pcff	Literature
CO_2/methyl lactate				
0	1	0.960	0.9055	0.8256
0.2	21	0.9570	0.9130	–
0.4	41	0.9441	0.9078	–
0.6	59	0.9328	0.8801	–
0.8	72	0.8755	0.7757	–
0.98	83	0.4792	0.1813	–

X_{CO_2}	p (bar)	COMPASS II	pcff	Universal	Literature
CO_2/ethyl lactate					
0	1	0.9601	0.9055	–	0.8214
0.2	18	0.9655	0.9163	0.9002	–
0.4	37	0.9431	0.8581	0.8923	–
0.6	55	0.9317	0.8443	0.8523	–
0.796	70	0.8923	0.7012	0.68534	–
0.97	83	0.5513	0.2416	0	–

X_{CO_2}	p (bar)	COMPASS II	pcff	Literature
CO_2/butyl lactate				
0	1	0.9601	0.9055	0.7479
0.2	15	0.9212	0.8775	–
0.4	32	0.9314	0.8332	–
0.6	51	0.9123	0.8166	–
0.798	70	0.8604	0.6861	–
0.98	84	0.1451	0.1983	–

Results have been calculated from literature values of ε

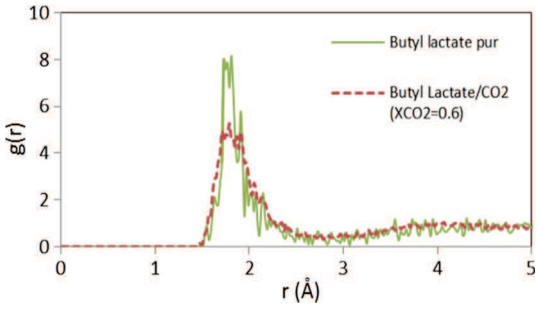

Fig. 11 Radial distribution function as a function of the distance for butyl lactate and CO_2 expanded lactate where $X_{CO_2} = 0.6$ {intermolecular $g(r)$ between the hydrogen of the hydroxyl group and the double bonded oxygen of the lactate}

4 Conclusions

As it has been presented, CO_2 has a great effect on alkyl lactate networks, which is evidenced by the decrease in π^* and α parameters of the three alkyl lactates studied; this behavior is expected to be reproduced by other members of the alkyl lactate family to a greater-or-lesser extent depending on the hydrocarbon chain length and/or the hydrocarbon chain branching. The solubility parameter and Kamlet–Taft (π^* and α) parameters decrease monotonically with CO_2 pressure as expected from the parameters of pure CO_2.

Packing fractions calculated from molecular modeling allowed us to observe that CO_2 is initially incorporated into the lactate's hydrogen bonding structure; then, after a certain composition, the solvent network is broken by the addition of CO_2. This behavior is observed as well in the density, which initially increases slightly at low concentrations of CO_2, but then decreases at higher concentrations of CO_2. These observations are attributed to the higher free volume present in expanded solvents than in non-expanded solvents. Hydrocarbon chain length has been observed to be a key factor in volumetric expansion and, as a consequence, in density changes as the density increases at low CO_2 pressures: butyl lactate > ethyl lactate > methyl lactate. The solubility of CO_2 in the alkyl lactate phase has been found to increase with the hydrocarbon's chain length.

The results presented in this study show that physicochemical properties can be significantly modulated by the CO_2 concentration, resulting from variation of the pressure, for the three studied members of the alkyl lactate family. The hydrocarbon chain length effect is an important factor to take into account when gas-expanded liquids are studied.

Acknowledgements Authors thank gratefully The Centre Informatique National de l'Enseignement Supérieur (CINES) for the permission to perform molecular dynamics calculations on the OCCIGEN supercomputer and their technical support for this project. This work was Granted access to the HPC resources of CINES under the allocation 2015-c2016087414 made by GENCI.

References

1. Gu, Y., Jerome, F.: Bio-based solvents: an emerging generation of fluids for the design of eco-efficient processes in catalysis and organic chemistry. Chem. Soc. Rev. **42**, 9550–9570 (2013)
2. Aparicio, S.: Computational study on the properties and structure of methyl lactate. J. Phys. Chem. A **111**, 4671–4683 (2007)
3. Pereira, C.S.M., Silva, V.M.T.M., Rodrigues, A.E.: Ethyl lactate as a solvent: properties, applications and production processes—a review. Green Chem. **13**, 2658–2671 (2011)
4. Dandia, A., Jain, A.K., Laxkar, A.K.: Ethyl lactate as a promising bio based green solvent for the synthesis of spiro-oxindole derivatives via 1,3-dipolar cycloaddition reaction. Tetrahedron Lett. **54**, 3929–3932 (2013)
5. Wan, J.-P., Wang, C., Zhou, R., Liu, Y.: Sustainable H_2O/ethyl lactate system for ligand-free Suzuki–Miyaura reaction. RSC Adv. **2**, 8789–8792 (2012)
6. Bennett, J.S., Charles, K.L., Miner, M.R., Heuberger, C.F., Spina, E.J., Bartels, M.F., Foreman, T.: Ethyl lactate as a tunable solvent for the synthesis of aryl aldimines. Green Chem. **11**, 166–168 (2009)
7. Akien, G.R., Poliakoff, M.: A critical look at reactions in class I and II gas-expanded liquids using CO_2 and other gases. Green Chem. **11**, 1083–1100 (2009)
8. Subramaniam, B.: Gas-expanded liquids for sustainable catalysis and novel materials: recent advances. Coord. Chem. Rev. **254**, 1843–1853 (2010)
9. Subramaniam, B.: Exploiting neoteric solvents for sustainable catalysis and reaction engineering: opportunities and challenges. Ind. Eng. Chem. Res. **49**, 10218–10229 (2010)
10. Medina-Gonzalez, Y., Tassaing, T., Camy, S., Condoret, J.-S.: Phase equilibrium of the CO_2/glycerol system: experimental data by in situ FT-IR spectroscopy and thermodynamic modeling. J. Supercrit. Fluids **73**, 97–107 (2013)

11. Gohres, J.L., Kitchens, C.L., Hallett, J.P., Popov, A.V., Hernandez, R., Liotta, C.L., Eckert, C.A.: A spectroscopic and computational exploration of the cybotactic region of gas-expanded liquids: methanol and acetone. J. Phys. Chem. B. **112**, 4666–4673 (2008)
12. Scurto, A.M., Hutchenson, K., Subramaniam, B.: Gas-expanded liquids: fundamentals and applications. In: Gas-Expanded Liquids and Near-Critical Media, pp. 1–3. American Chemical Society (2009)
13. Cho, D.W., Shin, J., Shin, M.S., Bae, W., Kim, H.: High-pressure phase behavior of propyl lactate and butyl lactate in supercritical carbon dioxide. J. Chem. Thermodyn. **47**, 177–182 (2012)
14. Cho, D.W., Shin, M.S., Shin, J., Bae, W., Kim, H.: High-pressure phase behavior of methyl lactate and ethyl lactate in supercritical carbon dioxide. J. Chem. Eng. Data **56**, 3561–3566 (2011)
15. Peng, D.Y., Robinson, D.B.: A new two-constant equation of state. Ind. Eng. Chem. Fundam. **15**, 59–64 (1976)
16. Perdew, J.P., Wang, Y.: Accurate and simple analytic representation of the electron-gas correlation energy. Phys. Rev. B **45**, 13244 (1992)
17. Vosko, S.H., Wilk, L., Nusair, M.: Accurate spin-dependent electron liquid correlation energies for local spin density calculations: a critical analysis. Can. J. Phys. **58**, 1200–1211 (1980)
18. Ortmann, F., Bechstedt, F., Schmidt, W.G.: Semiempirical van der Waals correction to the density functional description of solids and molecular structures. Phys. Rev. B. **73**, 205101 (2006)
19. Delley, B.: Ground-state enthalpies: evaluation of electronic structure approaches with emphasis on the density functional method. J. Phys. Chem. A **110**, 13632–13639 (2006)
20. Gohres, J.L., Popov, A.V., Hernandez, R., Liotta, C.L., Eckert, C.A.: Molecular dynamics simulations of solvation and solvent reorganization dynamics in CO_2-expanded methanol and acetone. J. Chem. Theory Comput. **5**, 267–275 (2009)
21. Chen, X., Yuan, C., Wong, C.Y., Zhang, G.: Molecular modeling of temperature dependence of solubility parameters for amorphous polymers. J. Mol. Model. **18**, 2333–2341 (2012)
22. Neumann, M., Steinhauser, O.: Computer simulation and the dielectric constant of polarizable polar systems. Chem. Phys. Lett. **106**, 563–569 (1984)
23. Sharma, M., Resta, R.: C.R.: Dipolar correlations and the dielectric permittivity of water. Phys. Rev. Lett. **98**, 247401 (2007)
24. Abbott, A.P., Hope, E.G., Mistry, R., Stuart, A.M.: Probing the structure of gas expanded liquids using relative permittivity, density and polarity measurements. Green Chem. **11**, 1530–1535 (2009)
25. Mistry, R.: Characterisation and Applications of CO_2-Expanded Solvents, Ph.D. thesis. Iniversity of Leicester (2008)
26. Kurniasih, I.N., Liang, H., Mohr, P.C., Khot, G., Rabe, J.P., Mohr, A.: Nile Red dye in aqueous surfactant and micellar solution. Langmuir **31**, 2639–2648 (2015)
27. Aparicio, S., Halajian, S., Alcalde, R., García, B., Leal, J.M.: Liquid structure of ethyl lactate, pure and water mixed, as seen by dielectric spectroscopy, solvatochromic and thermophysical studies. Chem. Phys. Lett. **454**, 49–55 (2008)
28. Li, H., Maroncelli, M.: Solvation and solvatochromism in CO_2-expanded liquids. 1. Simulations of the solvent systems CO_2 + cyclohexane, acetonitrile, and methanol. J. Phys. Chem. B **110**, 21189–21197 (2006)
29. Lomba, L., Giner, B., Zuriaga, E., Gascón, I., Lafuente, C.: Thermophysical properties of lactates. Thermochim. Acta **575**, 305–312 (2014)
30. Lomba, L., Rosa Pino, M., Lafuente, C., Carmen Lopez, M., Giner, B.: The $p\rho T$ behaviour of the lactate family. J. Chem. Thermodyn. **58**, 8–13 (2013)
31. Bondi, A.: van der Waals volumes and radii. J. Phys. Chem. **68**, 441–451 (1964)